Development of Space Charge and Growth of Ionization in the Transient Townsend Discharge

YASUNORI MIYOSHI
Nagoya Institute of Technology, Gokiso-Cho, Showa-Ku, Nagoya, Japan
(Received November 13, 1958; revised manuscript received September 25, 1959)

By using the general formulas derived from the analysis in a previous paper, calculations are made of the development of electronic and ionic space charges, the growth of space-charge-distorted field, the buildup of current, and the gain in ionization integral due to the field distortion in the transient Townsend discharge. On the basis of these data, two types of Townsend-mechanism spark breakdown are also discussed.

I. INTRODUCTION

TO explain the formation stage of spark breakdown, the development of electronic and ionic space charges and the growth of currents in a uniform field gap, after a step-function-like impulse voltage V has been applied, are calculated using the general formulas derived in the previous paper[1] (hereafter designated as PR1). The growth of the space-charge-distorted field and the increase of the Townsend ionization integral due to the field distortion are also calculated.

Several combinations of γ_i and γ_p—coefficients of electron emission by positive ion and photon at the cathode, respectively—are chosen to show the effect of secondary mechanisms on the buildup of discharge current.

The calculated results give an adequate estimate of the errors in employing the formulas of PR1 which ought to be approximately correct for (b) and (c) ranges.

The contents of this paper are an extension of the study initiated in PR1 and should be read in conjunction with PR1. These studies have made clear the realities of the development of space charge, space charge distortion of field, and the growth of ionization by collision of electrons in gases in the formative time of spark breakdown.

Numerical calculations are made under the following conditions:

air, $l=1$ cm, $p=722$ mm Hg;
sparking field: $E_s=28.5$ kv/cm;
second Townsend coefficient: $\gamma=\gamma_i+\gamma_p=1.5\times10^{-5}$;
electron velocity: $v_-=1.6\times10^7$ cm/sec;
positive-ion velocity: $v_+=8\times10^4$ cm/sec;
electron transit time: $t_-=l/v_-=6.25\times10^{-8}$ sec;
positive-ion transit time: $t_+=l/v_+=1.25\times10^{-5}$ sec;
resultant transit time: $\bar{t}=l/\bar{v}=t_-+t_+$.

These are similar to one of the gap conditions set in the experiments of Fisher and his collaborators[2] and of Bandel.[3]

All the respective symbols used in the present paper have the same meanings that they have in PR1. For example, the three time ranges are as follows:

(a) range: $0\leqq t\leqq t_-$,
(b) range: $t_-\leqq t\leqq \bar{t}$,
(c) range: $\bar{t}\leqq t$.

II. CHARACTERISTIC CONSTANTS

Characteristic constants λ_k for ranges (a), (b), and (c) which determine the temporal growth of Townsend discharge are the roots of Eqs. (a.3), (b.4), and (c.4) in PR1, respectively. From (a.3) and (a.5), we have[4]

$$\lambda_{a1}\cong\alpha\bar{v}(1+\gamma_i),\quad \lambda_{a2}\cong\alpha v_-(1+\gamma_p), \tag{1}$$

$$\nu_{a0}\cong1/(1+\gamma),\quad \nu_{a1}\cong\gamma_i/(1+\gamma),\quad \nu_{a2}\cong\gamma_p/(1+\gamma). \tag{2}$$

Real roots for (b) and (c) ranges, λ_{b1}, λ_{b2}, and λ_{c1} can be obtained graphically. Figures 1(a) and 1(b) show the roots thus obtained for various values of γ_i, γ_p, and percent overvoltage Δ. The characteristic constants for the special cases are summarized in Table I, where Λ is the real root of Eq. (A.1) in PR1.

As seen in the following chapters, modes of development of space charges, buildup of current, growth of space-charge-distorted field, and increase of ionization integral in the transient Townsend discharge can be classified into two distinguishable cases, that is γ_p-*predominant* cases and γ_i-*predominant* cases; the former belongs to $\lambda_{b1}>0$ and the latter, $\lambda_{b1}<0$. Figure 2 shows the two cases represented in γ_i, γ_p, and Δ planes.

TABLE I. Characteristic constants for the special cases.

	$\gamma=\gamma_p$	$\gamma=\gamma_i$
λ_{a1}	$\alpha\bar{v}$	$\alpha\bar{v}(1+\gamma)$
λ_{a2}	$\alpha v_-(1+\gamma)$	αv_-
λ_{b1}	$\alpha\bar{v}$[a] Λ/t_-[b]	$-\infty$
λ_{b2}	Λ/t_-[a] $\alpha\bar{v}$[b]	$\alpha\bar{v}(1+\gamma)$
λ_{c1}	Λ/t_-	$\Lambda/\bar{t}$

[a] Left column, under the condition $\gamma\{\exp[\alpha l(\bar{v}/v_+)]-1\}/(\bar{v}/v_+)>1$.
[b] Right column, under the condition $\gamma\{\exp[\alpha l(\bar{v}/v_+)]-1\}/(\bar{v}/v_+)<1$.

[1] Y. Miyoshi, Phys. Rev. **103**, 1609 (1956).
[2] L. H. Fisher and B. Bederson, Phys. Rev. **81**, 109 (1951), etc.
[3] H. W. Bandel, Phys. Rev. **95**, 1117 (1954).
[4] Y. Miyoshi, supplementary note to "Theoretical Analysis of Buildup of Current in Transient Townsend Discharge," Bull. Nagoya Inst. Technol. **9**, 95 (1957).

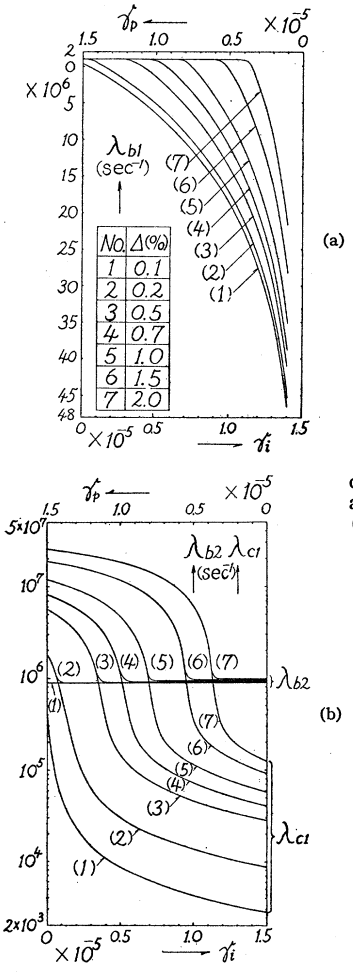

FIG. 1. Characteristic constants *vs* γ_i, γ_p with Δ as a parameter. (a) λ_{b1}. (b) λ_{b2} and λ_{c1}.

All the characteristics given in the following chapters are calculated for the case: $\Delta=1\%$. The buildup of transient Townsend discharge for other Δ values, however, could be measured to some extent from the characteristics obtained for the case where $\Delta=1\%$, because the effect of γ_i, γ_p, and Δ on the growth of discharge can be judged from Fig. 2.[5] The computed results for various Δ and gap conditions will be published in the future.

III. SPACE CHARGE DISTRIBUTION

Several examples of electronic and ionic streams, $N_-(x,t)$ and $N_+(x,t)$, or the electronic and ionic densities, $n_-(x,t)=N_-(x,t)/v_-$ and $n_+(x,t)=N_+(x,t)/v_+$, are shown in Figs. 3 and 4 as functions of x with t as a parameter. (The values of the parameter t for each curve in these figures is given in Table II.) In them, N_0 is the initial electron stream supplied externally at the cathode and $n_0=N_0/\bar{v}$. The electronic and ionic space charge densities in the (a) range are nearly independent of γ_i and γ_p as immediately inferred from Eqs. (1) and (2) in the preceding chapter; so n_- and n_+ in the (a) range are given only for the two special cases, $\gamma_i=0$ and $\gamma_p=0$ in the figures.

Figures 5(a) and 5(b) show $n_-(x,t_-)$ and $n_+(x,t_-)$, the electronic and ionic densities at the boundary between (a) and (b) ranges in the two extreme cases. The difference $\Delta n_-(x,t_-)$ between $n_-(x,t_-)$ from Eq. (a.6) and $n_-(x,t_-)$ from Eq. (b.9) as well as the difference $\Delta n_+(x,t_-)$ between $n_+(x,t_-)$ from Eq. (a.7) and $n_+(x,t_-)$ from Eq. (b.10A) gives the error in Eqs. (b.9), (b.10A), because Eqs. (a.6) and (a.7) are the exact solutions for $N_-(x,t)$ or $n_-(x,t)v_-$ and $N_+(x,t)$ or $n_+(x,t)v_+$ under the given initial condition. $\Delta n_-(x,t_-)$ and $\Delta n_+(x,t_-)$ are small and completely negligible in γ_i-predominant cases and almost negligible in γ_p-predominant cases, so the errors of Eqs. (b.9)–(b.13) in PR1 matter little and these finite-term solutions can be sufficiently useful for the computation of the transient Townsend discharge. Since the finite-term solutions become more accurate

TABLE II. Values of the parameter t (in seconds) for the curves in Figs. 3 and 4.

Curve	(a)	(b)	(c)	(d)
γ_i ($\times10^{-5}$)	0	0.6	0.9	1.5
γ_p ($\times10^{-5}$)	1.5	0.9	0.6	0
	A_1, $(0.1t_-)$			A_1, $(0.1t_-)$
	A_2, $(0.2t_-)$			A_2, $(0.2t_-)$
	A_3, $(0.3t_-)$			A_3, $(0.3t_-)$
	A_4, $(0.4t_-)$			A_4, $(0.4t_-)$
	A_5, $(0.5t_-)$			A_5, $(0.5t_-)$
	A_6, $(0.6t_-)$			A_6, $(0.6t_-)$
	A_7, $(0.7t_-)$			A_7, $(0.7t_-)$
	A_8, $(0.8t_-)$			A_8, $(0.8t_-)$
	A_9, $(0.9t_-)$			A_9, $(0.9t_-)$
	A_{10}, B_1, (t_-)	B_1, (t_-)	B_1, (t_-)	A_{10}, B_1, (t_-)
		B_2, 6.8×10^{-8}		B_2, 7×10^{-8}
		B_3, 8×10^{-8}		
	B_2, 1×10^{-7}	B_4, 1×10^{-7}		B_3, 1×10^{-7}
	B_3, 2×10^{-7}			B_4, 2×10^{-7}
	B_4, 3×10^{-7}	B_5, 3×10^{-7}	B_2, 3×10^{-7}	B_5, 3×10^{-7}
	B_5, 5×10^{-7}	B_6, 5×10^{-7}		B_6, 5×10^{-7}
		B_7, $(10t_-)$	B_3, $(10t_-)$	
	B_6, 7×10^{-7}			B_7, 7×10^{-7}
		B_8, 8×10^{-7}		
	B_7, 1×10^{-6}	B_9, 1×10^{-6}		B_8, 1×10^{-6}
	B_8, 2×10^{-6}			B_9, 2×10^{-6}
		B_{10}, 3×10^{-6}	B_4, 3×10^{-6}	B_{10}, 3×10^{-6}
		B_{11}, 5×10^{-6}		B_{11}, 5×10^{-6}
		B_{12}, $(100t_-)$	B_5, $(100t_-)$	
				B_{12}, 7×10^{-6}
		B_{13}, 8×10^{-6}	B_6, 8×10^{-6}	
		B_{14}, 1×10^{-5}	B_7, 1×10^{-5}	B_{13}, 1×10^{-5}
			B_8, 1.1×10^{-5}	
		B_{15}, 1.2×10^{-5}		
		B_{16}, $(\bar{t})$	B_9, C_1, $(\bar{t})$	B_{14}, C_1, $(\bar{t})$
				C_2, 2×10^{-5}
			C_2, $(2\bar{t})$	
				C_3, 3×10^{-5}
				C_4, 5×10^{-5}
			C_3, 6×10^{-5}	
				C_5, 7×10^{-5}
			C_4, 1×10^{-4}	C_6, 1×10^{-4}
			C_5, $(10\bar{t})$	
			C_6, 1.6×10^{-4}	
			C_7, 2×10^{-4}	C_7, 2×10^{-4}
				C_8, 3×10^{-4}
				C_9, 5×10^{-4}

[5] For extremely small percent overvoltage, formative time lags extend to the (c) range even in the cases $\gamma\cong\gamma_p$. Such cases will be discussed in other papers.

as t increases,[6] Eqs. (b.9)–(b.13) will be precise for larger t of the (b) range. Especially, in γ_i-predominant cases, they could be an exact solution for the later stage of the (b) range. In γ_p-predominant cases, space charge accumulation enough to propagate a streamer or a conducting plasma from the anode is reached in some t_- or some tens of t_-, the time required being the formative time of spark under the application of an overvoltage. In such cases, Eqs. (b.9)–(b.13) are sufficiently useful for calculation of the later stage of formative time of spark; of course, it is not necessary to calculate the next (c) range. On the contrary, in γ_i-predominant cases, a considerable space charge concentration to distort the field across the gap is attained not within the (b) range, but in the (c) range under the application of an overvoltage. In such cases, a further calculation of the (c) range is needed and the continuity of electronic and ionic distributions at the boundary between the (b) and (c) ranges becomes a subject of discussion.

Figures 6(a) and 6(b) show $n_-(x,\bar{t})$ and $n_+(x,\bar{t})$, the charge densities at the boundary between the (b) and (c) ranges. The difference $\Delta n_-(x,\bar{t})$ between $n_-(x,\bar{t})$ from Eq. (b.9) and $n_-(x,\bar{t})$ from Eq. (c.8) as well as the difference $\Delta n_+(x,\bar{t})$ between $n_+(x,\bar{t})$ from Eq. (b.10B) and $n_+(x,\bar{t})$ from Eq. (c.9) may not be overlooked. Our approximate solutions, however, become more accurate as t increases in the same way as in the (b) range; hence, Eqs. (c.8)–(c.12) are also useful for the calculation of the later stage of spark formation.

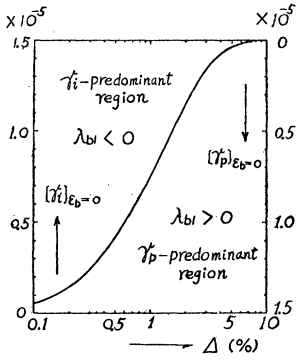

FIG. 2. γ_i-predominant and γ_p-predominant regions represented in γ_i, γ_p, and Δ plane.

Space distributions of n_- for the (b) and (c) ranges are nearly exponential in x. This is true especially for γ_i-predominant cases because $\lambda_{b1}/v_- \ll \lambda_{b2}/v_- \ll \alpha$ and $\lambda_{c1}/v_- \ll \alpha$. For the n_- distribution,[7]

$$N_-(x,t)/N_0 = n_-(x,t)/n_0 \cdot (v_-/\bar{v}) = \begin{cases} e^{\alpha x}\sum \nu_{bk} \exp\lambda_{bk}(t-x/v_-) \sim \propto e^{\alpha x} & \text{for the (b) range} \\ e^{\alpha x}\sum \nu_{ck} \exp\lambda_{ck}(t-x/v_-) \sim \propto e^{\alpha x} & \text{for the (c) range.} \end{cases} \quad (3)$$

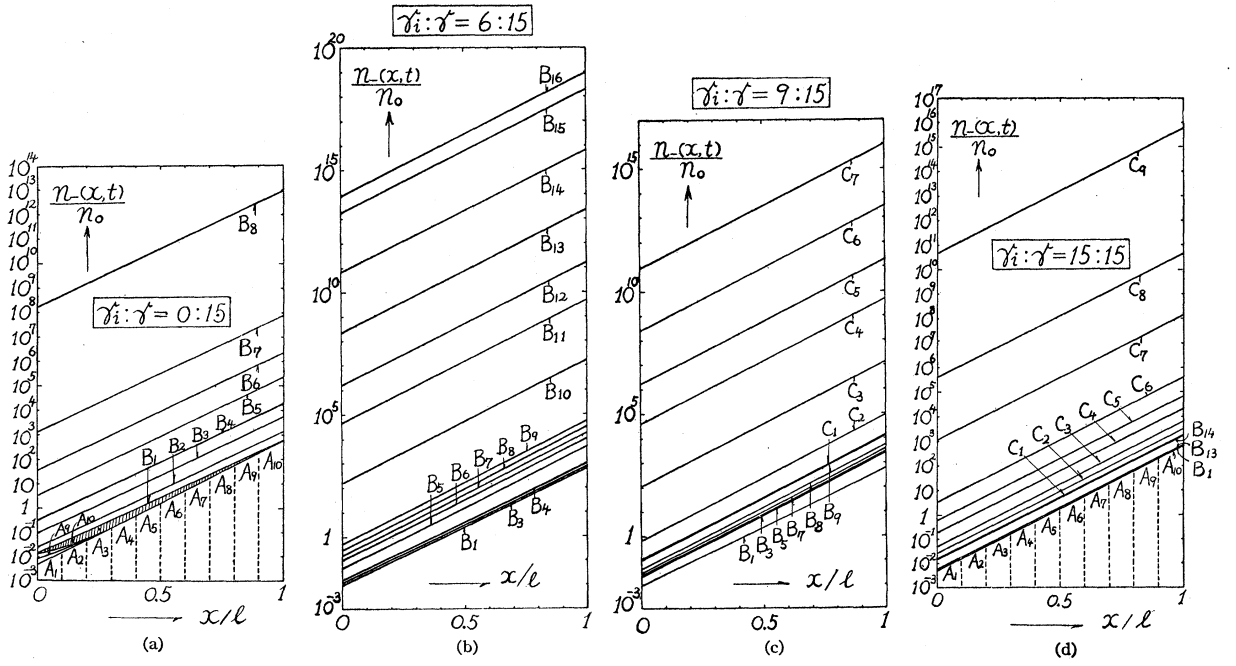

FIG. 3. Electron distribution in transient Townsend discharge. (a) $\gamma_i=0$, $\gamma_p=1.5\times10^{-5}$; (b) $\gamma_i=0.6\times10^{-5}$, $\gamma_p=0.9\times10^{-5}$; (c) $\gamma_i=0.9\times10^{-5}$, $\gamma_p=0.6\times10^{-5}$; (d) $\gamma_i=1.5\times10^{-5}$, $\gamma_p=0$. See Table II for explanation of the curve parameter.

[6] See the Appendix of PR1 and another paper (unpublished).
[7] $\sim\propto$ denotes "nearly proportional."

For the n_+ distribution,[7]

$$N_+(x,t)/N_0=n_+(x,t)/n_0\cdot(v_+/\bar{v})$$

$$=\begin{cases} e^{\alpha x}\sum\left(\dfrac{\alpha}{\phi_{bk}}-\nu_{bk}\right)\exp\lambda_{bk}(t-x/v_-)\sim\propto e^{\alpha x} \\ \qquad \text{for} \quad x\leqq v_+(\bar{t}-t) \quad \text{of the (b) range}, \\ \sum\left(\dfrac{\alpha}{\phi_{bk}}-\nu_{bk}\right)\exp\lambda_{bk}(t-x/v_-) \\ \quad\times\{e^{\alpha l}\exp\lambda_{bk}(x-l)/\bar{v}-e^{\alpha x}\}\sim\propto(e^{\alpha l}-e^{\alpha x}) \\ \qquad \text{for} \quad x\cong l \qquad \text{of the (b) range}, \\ \sum\left(\dfrac{\alpha}{\phi_{ck}}-\nu_{ck}\right)\exp\lambda_{ck}(t-x/v_-) \\ \quad\times\{e^{\alpha l}\exp\lambda_{ck}(x-l)/\bar{v}-e^{\alpha x}\}\sim\propto(e^{\alpha l}-e^{\alpha x}) \\ \qquad \text{for} \quad x\cong l \qquad \text{of the (c) range}. \end{cases} \tag{4}$$

Consequently, the electronic space charges develop a distribution similar to the steady-state one already in an early stage of formative time of spark but it does not apply to the ionic space charges.

IV. STREAM AND CURRENT

$N_-(0,t)$ or $n_-(0,t)$, $N_+(0,t)$ or $n_+(0,t)$, $N_-(l,t)$ or $n_-(l,t)$, $J_-(t)$ or $N_p(t)$,[1] and $J_+(t)$ for various combinations of γ_i and γ_p are shown in Figs. 7–11. The curve parameters, γ_i and γ_p for the figures in Chaps. IV-VIII (Figs. 7-15, 17-24) are those given in the accompanying Table III. All the characteristics shown in these figures indicate that they can be classified in two groups of γ_p-predominant cases ($\lambda_{b1}>0$) and γ_i-predominant cases ($\lambda_{b1}<0$). As the development of space charges in the preceding chapter has indicated, the charge streams or currents large enough to drive the discharge into the more advanced form, "glow" or "arc," are attained in the (b) range for the former group of $\lambda_{b1}>0$ and in the (c) range for the latter group of $\lambda_{b1}<0$.

Moreover, as expected from the results for the space charge distribution, $N_+(0,t)$ and other functions, except $N_-(0,t)$ or $n_-(0,t)$, are not continuous when $t=t_-$ and $t=\bar{t}$; but the discontinuity of $N_+(0,t)$ when $t=t_-$ is negligibly small for γ_i-predominant cases and not serious for γ_p-predominant cases. Though the discontinuity of $N_+(0,t)$ when $t=\bar{t}$ could not be neglected, it gradually approaches an exact solution with t. For this reason, $J_-(t)$ or $N_p(t)$, $J_+(t)$, and other related quantities which will be referred to afterwards—e.g., $\gamma_iN_+(0,t)$, $\gamma_pN_p(t)$— are described to be continuous at t_- or $\bar{t}$ and to approach smoothly to the later characteristic which may be regarded as accurate.

TABLE III. Values of the parameters γ_i and γ_p for the curves in Figs. 7–15 and Figs. 17–24.

No.	(i)	(ii)	(iii)	(iv)	(v)	(vi)	(vii)	(viii)	(ix)	(x)
$\gamma_i(\times10^{-6})$	0	1	2	4	6	9	11	13	14	15
$\gamma_p(\times10^{-6})$	15	14	13	11	9	6	4	2	1	0

The effect of positive ions and photons at the cathode on the buildup of current in the transient Townsend discharge is measured straightforwardly by $\gamma_iN_+(0,t)$ and $\gamma_pN_p(t)$, respectively, but not by the magnitudes of γ_i and γ_p. Figure 12 shows that such quantities $\gamma_iN_+(0,t)$ and $\gamma_pN_p(t)$ increase with t for several values of γ_i and γ_p. It should be noted that $\gamma_pN_p(t)$ leads $\gamma_iN_+(0,t)$ throughout in γ_p-predominant cases, but $\gamma_iN_+(0,t)$ begins to lead $\gamma_pN_p(t)$ at the last stage of the (b) range or the initial stage of the (c) range in γ_i-predominant cases. That is, at the last stage of formative time of spark breakdown, $\gamma_pN_p(t)\gg\gamma_iN_+(0,t)$ in γ_p-predominant cases and $\gamma_pN_p(t)\lesssim\gamma_iN_+(0,t)$ in γ_i-predominant cases.

From these numerical calculations, it also follows that charge streams at the cathode or at the anode increase nearly proportional to $J(t)$, the total current density, except for smaller values of J (Figs. 13–15). In these characteristics, the relation between the quantities concerning electrons and J is in opposite phase to that of the quantities concerning positive ions and J with respect to the effect of secondary processes.

V. SPACE CHARGE DISTORTION OF FIELD

Electronic and ionic densities, $n_-(x,t)$ and $n_+(x,t)$, develop progressively in a formative time of spark as shown in Chap. III. Then the space charge density,[8]

$$\rho(x,t)=en(x,t)=e\{n_+(x,t)-n_-(x,t)\}, \tag{5}$$

as well as the space charge distortion of field grows rapidly. The actual field $E(x,t)$ in the gap is the sum of the applied field $\bar{E}=V/l$ and the distorted field $\Delta_\rho E(x,t)$ due to the space charge $\rho(x,t)$. $E(x,t)$ or $\Delta_\rho E(x,t)$ can easily be determined from the following equations[9]:

$$\text{Poisson's equation:} \quad dE/dx=-\rho/K; \tag{6}$$

$$\text{boundary condition:} \quad \int_0^l Edx=V. \tag{7}$$

That is,

$$\Delta_\rho E(x,t)=\frac{1}{l}\int_0^l\int_0^x\frac{\rho(x,t)}{K}dx^2-\int_0^x\frac{\rho(x,t)}{K}dx, \tag{8}$$

or

$$\frac{\Delta_\rho E}{E_0}=Q(1,t)-P\left(\frac{x}{l},t\right), \tag{9}$$

[8] e is the electronic charge.

[9] E is taken inversely to the x direction. V is assumed constant in this chapter. $K=1/4\pi$ for cgs esu; $K=\epsilon_0=8.854\times10^{-12}$ (farad/m) for mks units.

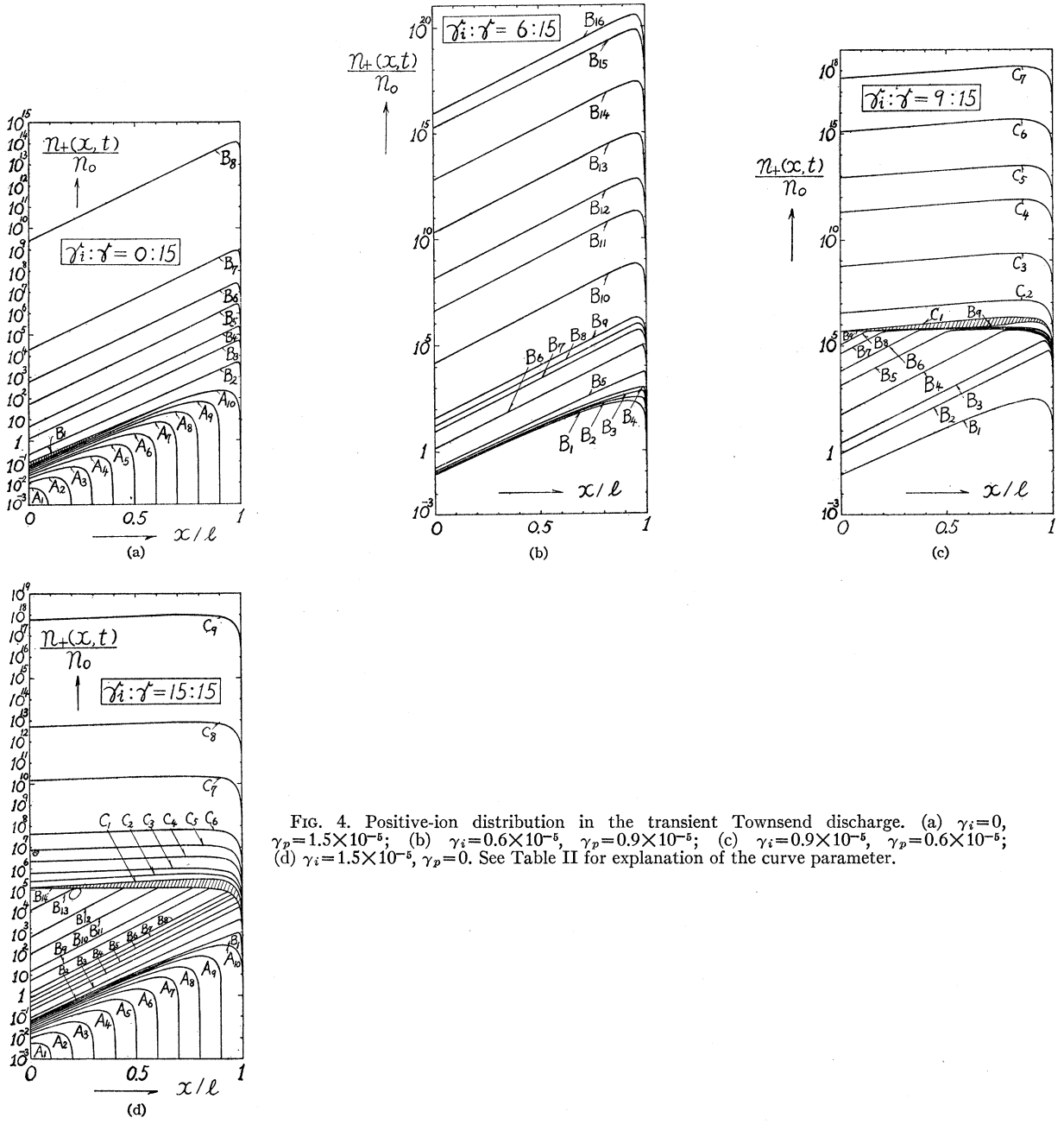

FIG. 4. Positive-ion distribution in the transient Townsend discharge. (a) $\gamma_i=0$, $\gamma_p=1.5\times10^{-5}$; (b) $\gamma_i=0.6\times10^{-5}$, $\gamma_p=0.9\times10^{-5}$; (c) $\gamma_i=0.9\times10^{-5}$, $\gamma_p=0.6\times10^{-5}$; (d) $\gamma_i=1.5\times10^{-5}$, $\gamma_p=0$. See Table II for explanation of the curve parameter.

where

$$P\left(\frac{x}{l},t\right)=\int_0^{x/l}\frac{n(x,t)}{n_0}d\left(\frac{x}{l}\right),$$

$$Q(1,t)=\int_0^1 P\left(\frac{x}{l},t\right)d\left(\frac{x}{l}\right), \tag{10}$$

$$E_0=en_0l/K.$$

Figure 16 shows the distribution of space-charge-distorted field $\Delta_pE(x,t)$ growing with t, obtained for the two special cases, $\gamma_i=0$ and $\gamma_p=0$. The values of the parameter t and the multiplication factors for the scales of the ordinate are listed in Table IV. For various values of γ_i and γ_p, the distorted field $\Delta_pE(0,t)$ at the cathode and $\Delta_p(x_0,t)$ at the plasma $[x=x_0]$ are given in Figs. 17 and 18 as functions of t and in Figs. 19 and 20 as functions of J. These distorted fields increase nearly proportionally to J except for the smaller values of J. $|\Delta_pE(x_0,t)|$ is always greater than $\Delta_pE(0,t)$ and a little greater than $|\Delta_pE(l,t)|$; but they become nearly equal to each other in several ion transit times for γ_i-predominant cases.

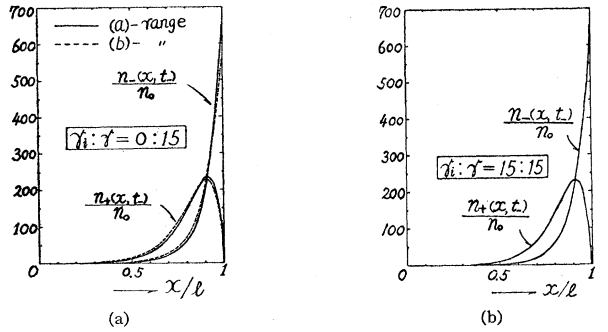

FIG. 5. Comparison of space charge distributions at t_- calculated from the (a)- and (b)-range solutions. Full line: calculated from the (a)-range solution, Eq. (a.6). Dotted line: calculated from the (b)-range solution, Eq. (b.9). (a) $\gamma_i=0$, $\gamma_p=1.5\times10^{-5}$; (b) $\gamma_i=1.5\times10^{-5}$, $\gamma_p=0$.

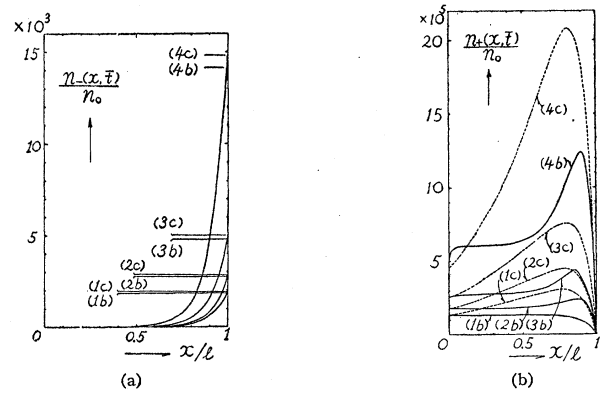

FIG. 6. Comparison of space charge distributions at $\bar{t}$ calculated from the (b)- and (c)-range solutions for γ_i-predominant cases. (1b)–(4b): calculated from (b)-range solutions, Eq. (b.9) and Eq. (b.10B). (1c)–(4c): calculated from (c)-range solutions, Eq. (c.8) and Eq. (c.9). (1b), (1c): $\gamma_i=1.5\times10^{-5}$, $\gamma_p=0$; (2b), (2c): $\gamma_i=1.3\times10^{-5}$, $\gamma_p=0.2\times10^{-5}$; (3b), (3c): $\gamma_i=1.1\times10^{-5}$, $\gamma_p=0.4\times10^{-5}$; (4b), (4c): $\gamma_i=0.9\times10^{-5}$, $\gamma_p=0.6\times10^{-5}$. (a) Electron distribution. (b) Positive-ion distribution.

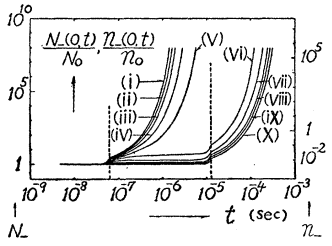

FIG. 7. Cathode electron stream $N_-(0,t)$ and cathode electron density $n_-(0,t)$ *vs* t. See Table III for explanation of the curve parameter.

The aforementioned x_0 is a position where the space charge concentration is zero:

$$\rho(x_0,t)=0;\quad n_-(x_0,t)=n_+(x_0,t);$$

hence its neighborhood ($x\cong x_0$) forms a plasma and $|\Delta_\rho E|$ has a maximum at that point.

VI. INCREASE OF IONIZATION INTEGRAL DUE TO SPACE-CHARGE DISTORTION

As the space-charge-field distortion develops, the Townsend ionization integral $\sigma=\int_0^l\alpha dx$ will increase. Using the expression $\alpha/p=A\{E/p-B\}^2$ in the same way as in PR1, the increment of the ionization integral can be determined as follows:

$$\Delta_\rho\sigma(t)=\int_0^l\alpha(E)dx-\alpha(\bar{E})l$$

$$=\frac{A}{p}\int_0^l\{\Delta_\rho E(x,t)\}^2dx, \tag{11}$$

or

$$\frac{\Delta_\rho\sigma}{\sigma_1}=\int_0^1\left\{\frac{\Delta_\rho E}{E_0}\right\}^2d\left(\frac{x}{l}\right), \tag{12}$$

where

$$\sigma_1=(\bar{\alpha}l)\left\{\frac{E_0/p}{\bar{E}/p-B}\right\}^2=\frac{AlE_0^2}{p}, \tag{13}$$

$$\bar{\alpha}=\alpha(\bar{E}).$$

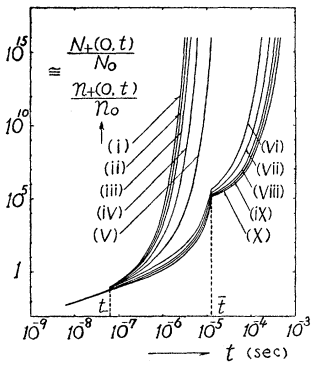

FIG. 8. Cathode ion stream $N_+(0,t)$ and cathode ion density $n_+(0,t)$ *vs* t. See Table III for explanation of the curve parameter.

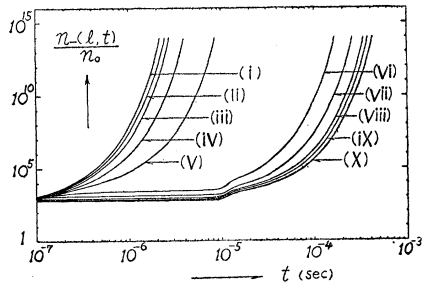

FIG. 9. Anode electron density $n_-(l,t)$ *vs* t. See Table III for explanation of the curve parameter.

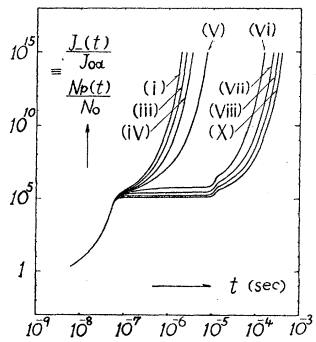

FIG. 10 Electron current density $J_-(t)$ or number of ionization chances $N_p(t)$ *vs* t. See Table III for explanation of the curve parameter.

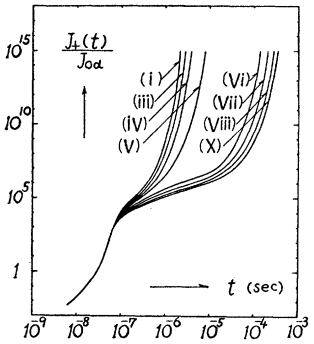

FIG. 11. Positive-ion current density $J_+(t)$ *vs* t. See Table III for explanation of the curve parameter.

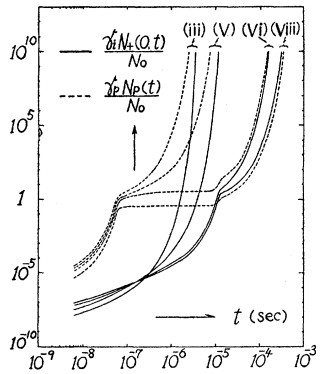

FIG. 12. Electron emissions by positive ions and photons at the cathode, $\gamma_i N_+(0,t)$ and $\gamma_p N_p(t)$ *vs* t. See Table III for explanation of the curve parameter.

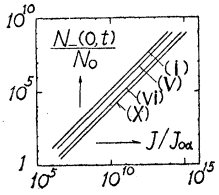

FIG. 13. Cathode electron stream $N_-(0,t)$ *vs* total current density J. See Table III for explanation of the curve parameter.

Figure 21 shows the increase of the integral $\Delta_\rho\sigma(t)$ due to space-charge distortion of field as a function of t for various values of γ_i and γ_p. Figure 22, showing the relation between $\Delta_\rho\sigma$ and J, indicates that $\Delta_\rho\sigma$ increases nearly proportionally to the square of J. This result is in accord with Bandel's in form.

VII. DECREASE OF IONIZATION INTEGRAL DUE TO FLOW OF CURRENT

So far the problem has been concerned with charge densities n_-, n_+, and n as well as current densities J_-, J_+, and J, but in the present chapter it is related directly to the external current $I=JS$; S is the discharge area in which the discharge is assumed to spread uniformly. Now we will discuss an influence of the decrease of gap voltage V caused by flow of current $I(t)$ on the ionization growth.[10,11]

[10] If we employ a condenser of relatively large capacity for a dc source, lowering of the source voltage due to flow of discharge current does not enter as in Bandel's experiments.

[11] It is clear from Mori's experiments (to be published in Electro-Technical Journal of Japan) on a spark at low pressure in air that larger series resistance causes less rapid buildup of the transient Townsend discharge and longer formative time lag of spark.

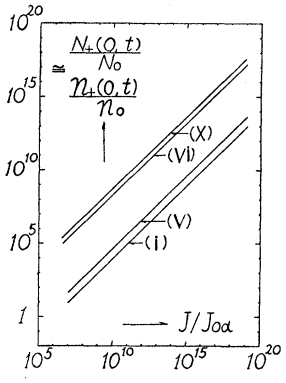

FIG. 14. Cathode ion stream $N_+(0,t)$ *vs* total current density J. See Table III for explanation of the curve parameter.

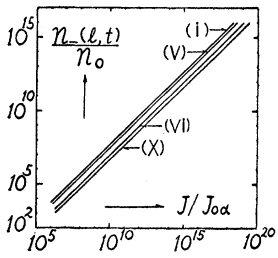

FIG. 15. Anode electron density $n_-(l,t)$ *vs* total current density J. See Table III for explanation of the curve parameter.

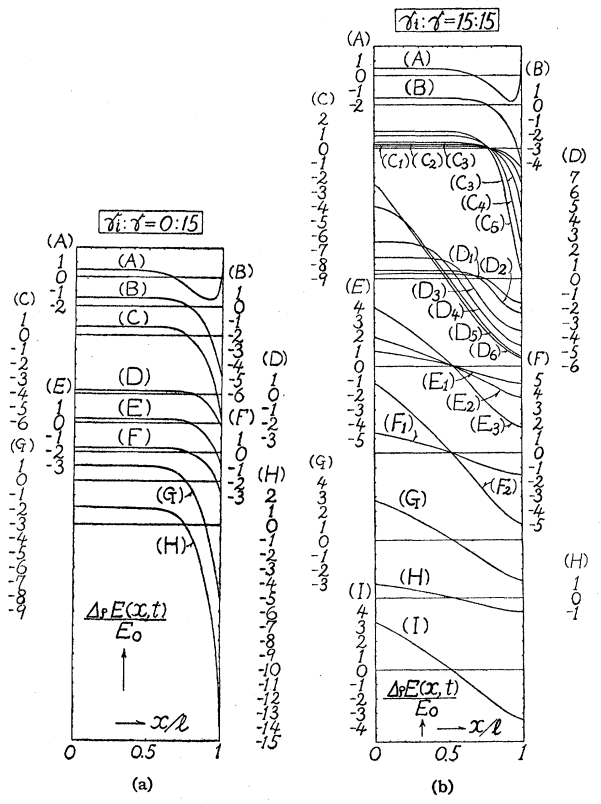

FIG. 16. Distribution of space-charge-distorted field $\Delta_\rho E(x,t)$ in the transient Townsend discharge. (a) $\gamma_i=0$, $\gamma_p=1.5\times10^{-5}$; (b) $\gamma_i=1.5\times10^{-5}$, $\gamma_p=0$. See Table IV for explanation of the curve parameter and the multiplication factor.

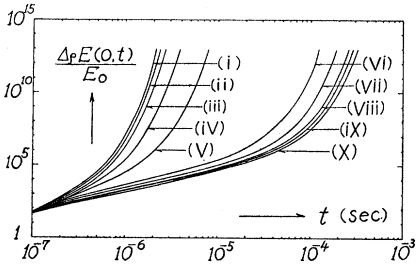

FIG. 17. Space-charge-distorted field at the cathode $\Delta_p E(0,t)$ *vs* t. See Table III for explanation of the curve parameter.

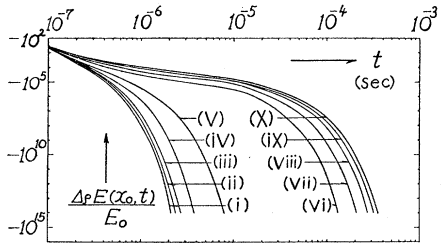

FIG. 18. Space-charge-distorted field at the plasma $\Delta_p E(x_0,t)$ *vs* t. See Table III for explanation of the curve parameter.

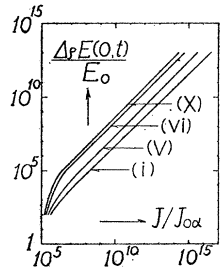

FIG. 19. Space-charge-distorted field at the cathode $\Delta_p E(0,t)$ *vs* total current density J. See Table III for explanation of the curve parameter.

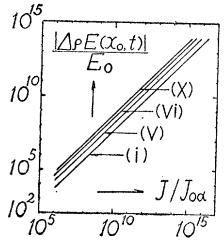

FIG. 20. Space-charge-distorted field at the plasma $\Delta_p E(x_0,t)$ *vs* total current density J. See Table III for explanation of the curve parameter.

The decrease of applied electric field in the gap owing to the potential drop in a series resistance R is

$$\Delta_I E = RI/l, \tag{14}$$

and the decrement of the Townsend ionization integral due to the potential drop is

$$\begin{aligned}\Delta_I\sigma(t) &= \alpha(\bar{E})l - \alpha(\bar{E}-\Delta_I E)l \\ &= 2Al\{\bar{E}/p - B\}\Delta_I E(t) - \frac{Al}{p}\{\Delta_I E(t)\}^2 \\ &\cong 2Al\{\bar{E}/p - B\}\Delta_I E(t),\end{aligned} \tag{15}$$

since $\Delta_I E$ can be neglected in comparison with $2\{\bar{E}-Bp\}$ for small values of I. Therefore

$$\Delta_I\sigma/\sigma_2 = J/J_{0\alpha}, \tag{16}$$

where

$$\sigma_2 = (\bar{\alpha}l)\frac{2J_{0\alpha}\{S/pl\}}{\{\bar{E}/p-B\}} = \frac{2J_0\{S/pl\}}{\{\bar{E}/p-B\}}, \tag{17}$$

$$J_0 = eN_0, \quad J_{0\alpha} = J_0/\alpha l.$$

Figure 23 shows the decrement of the ionization integral $\Delta_I\sigma(t)$ due to flow of current in the external circuit as a function of t for various values of γ_i and γ_p. It is the same as the relation between $J(t)$ and t as evident from Eq. (16).

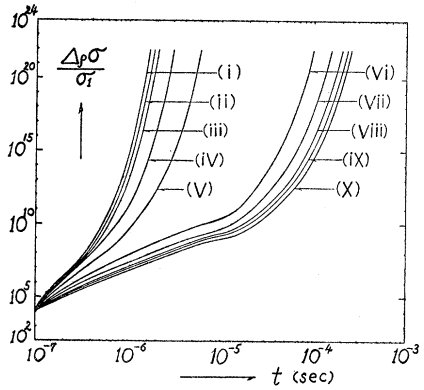

FIG. 21. Increment of ionization integral $\Delta_p\sigma(t)$ due to space-charge distortion of field *vs* t. See Table III for explanation of the curve parameter.

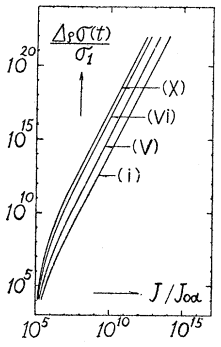

FIG. 22. Increment of ionization integral $\Delta_p\sigma(t)$ due to space-charge distortion of field *vs* total current density J. See Table III for explanation of the curve parameter.

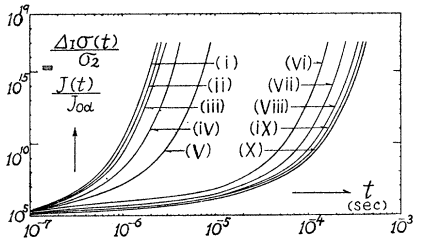

FIG. 23. Decrement of ionization integral $\Delta_I\sigma(t)$ due to potential drop in an external resistance *vs* t. See Table III for explanation of the curve parameter.

VIII. GROWTH OF IONIZATION

Since the space-charge accumulation and current are not large in the formative time of spark excepting its last stage, the increment $\Delta\sigma$ of the ionization integral can be expressed as the simple sum of $\Delta_p\sigma$ and $-\Delta_I\sigma$, that is

$$\Delta\sigma=\Delta_p\sigma-\Delta_I\sigma. \tag{18}$$

This is shown in Fig. 24 for several combinations of γ_i and γ_p. $\Delta_I\sigma$ is nearly proportional to J and $\Delta_p\sigma$, to J^2, so $\Delta\sigma$ is affected by the potential drop due to current flow more than by the space-charge effect in the earlier stage of the formative time lag, but later, the reverse holds. Hence

$$\begin{aligned}\Delta\sigma(t)&<0 \quad \text{for} \quad t<T_0\\ &=0 \quad \text{for} \quad t=T_0\\ &>0 \quad \text{for} \quad t>T_0.\end{aligned} \tag{19}$$

T_0 is a time when $\Delta\sigma$ becomes zero and obviously it is a function of γ_i and γ_p; when γ_i is larger, T_0 is also larger. Both in γ_i-predominant cases and γ_p-predominant cases, $\Delta\sigma$ increases faster from an instant close to T_0 and as a consequence, the discharge begins to develop the more advanced form—"glow." So T_0 is thought to be a time closely connected with the formative time as will be discussed in the next chapter.

$\Delta_p\sigma$ or $\Delta_I\sigma$, J, and I at time T_0, taking[12] $R=1000$ ohms and $S=S_0=78.5$ cm^2 (S_0 is the electrode area), are shown in Fig. 25; they decrease as γ_i increases while T_0 increases.

IX. TWO TYPES OF TOWNSEND-MECHANISM SPARK BREAKDOWN

In the last stage of formative time of spark, electronic and ionic space charge distributions in the whole gap, $n_-(x,t)$ and $n_+(x,t)$, are similar to those of the anode region of glow discharge in γ_p-predominant cases, and to those of the cathode region of glow discharge in γ_i-predominant cases. To be more precise, the space-charge distributions in the transient Townsend discharge at the time when the current density J comes near a critical value J_s necessary for the discharge to transit into complete breakdown, are as follows:

(I) γ_p-predominant cases

$$n_-(x,t)<n_+(x,t) \quad \text{for} \quad x<x_0, \tag{Ia}$$

$$n_-(x,t)>n_+(x,t) \quad \text{for} \quad x>x_0. \tag{Ib}$$

(II) γ_i-predominant cases

$$n_-(x,t)\ll n_+(x,t) \quad \text{for} \quad x<x_0, \tag{IIa}$$

$$n_-(x,t)>n_+(x,t) \quad \text{for} \quad x>x_0. \tag{IIb}$$

The region $x>x_0$ is very narrow, and the region $x<x_0$ covers almost the whole gap.

In γ_p-predominant cases, the region $x<x_0$ resembles the positive column where n_+ are slightly larger than n_- from (Ia), and the region $x>x_0$, the anode dark space from (Ib). In γ_i-predominant cases, on the other hand, the region $x<x_0$ resembles the cathode dark space where n_+ are much larger than n_- from (IIa), and the region $x>x_0$, the negative glow from (IIb). Consequently it may be said that in the Townsend-mechanism breakdown, the formative time is a preliminary stage for developing the anode region of glow discharge—*anodic breakdown*—in γ_p-predominant cases, and for developing the cathode region of glow discharge—*cathodic breakdown*—in γ_i-predominant cases.

TABLE IV. Values of the parameter t and the multiplication factors for the scales of the ordinates of the curves in Fig. 16.

(a)	(b)	multiplication factor	(a)	(b)	t (sec)
A	A	10	A	A	(t_-)
B	B	10^2	B	B	1×10^{-7}
C	C	10^3	C	C_1	2×10^{-7}
D	D	10^4	D	C_2	3×10^{-7}
E	E	10^5	E	C_3	5×10^{-7}
F	F	10^6	F	C_4	7×10^{-7}
G	G	10^7	G	C_5	1×10^{-6}
	H	10^{10}	H	D_1	2×10^{-6}
H	I	10^{12}		D_2	3×10^{-6}
				D_3	5×10^{-6}
				D_4	7×10^{-6}
				D_5	1×10^{-5}
				D_6 }	($\bar{t}$)
				E_1 }	
				E_2	2×10^{-5}
				E_3	3×10^{-5}
				F_1	5×10^{-5}
				F_2	7×10^{-5}
				G	1×10^{-4}
				H	2×10^{-4}
				I	3×10^{-4}

[12] The same as Bandel's excepting $R=2.1$ kilohms.

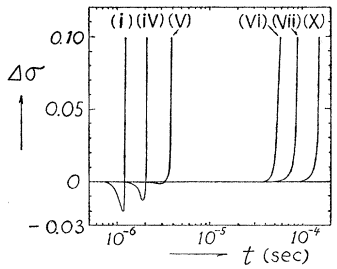

FIG. 24. Resultant increment of ionization integral $\Delta\sigma(t)$ *vs* t. See Table III for explanation of the curve parameter.

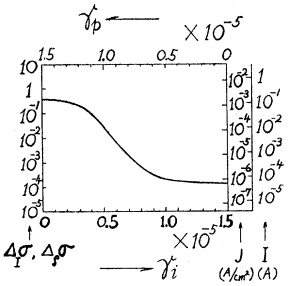

FIG. 25. Ionization integral, current and current density at the time T_0 *vs* γ_i, γ_p.

On the other hand, it is seen from Fig. 25 that the condition $\Delta\sigma=0$ at T_0 is attained at a higher current density in γ_p-predominant cases and at a lower current density in γ_i-predominant cases. Therefore it is known also that the same condition is attained at a higher current in the former cases and at a lower current in the latter if the discharge spreads completely over the whole electrode surfaces.

In γ_i-predominant cases, during the time $t<T_0$, $\Delta\sigma$ is as small in magnitude as the change in σ due to the fluctuation of electric source voltage still unavoidable by the present technique; hence the discharge is not brought to extinction, though the buildup of current becomes less rapid owing to negative $\Delta\sigma$. The characteristics common to current-time curves obtained by Bandel—more or less exponential increase of current in the middle of the time lag between the initial rapid buildup and the final upward-curving—may be explained as the result of σ being somewhat lowered by $\Delta_I\sigma$ in the middle period rather than by other causes. Conversely, in γ_p-predominant cases, it results from Fig. 24 that $\Delta\sigma$ is not so small in magnitude but it reaches a sufficiently negative value to hinder the growth of the discharge in $t<T_0$. On comparing $I(T_0)$ in Fig. 25 with Bandel's actual data for cases in which sparks just failed to develop (Figs. 2 and 5 in his paper) and other data of critical current just before breakdown obtained from static characteristics, our computed results seem to be rigorous for γ_i-predominant cases but not for γ_p-predominant cases. Such inconsistency, however, may be based on assuming that the discharge spreads over the whole surface of each electrode also in γ_p-predominant cases. Really, the transient Townsend discharge must be not much larger in sectional area than in an externally irradiated area in γ_p-predominant cases because the absorption of photons in gas permits in less degree photons to reach other parts of the cathode surface of longer path than the path to the externally irradiated part and also because the formative time is too short to spread the discharge over the whole surface of the electrode due to electronic diffusion. In γ_i-predominant cases, on the contrary, it spreads over the entire surfaces of the electrodes owing to electronic and ionic diffusion as in the case treated by Bandel.

Consequently,

$$S\ll S_0, \quad \text{for } \gamma_p\text{-predominant cases,}$$

$$S\cong S_0, \quad \text{for } \gamma_i\text{-predominant cases.}$$

The absorption of such photons as play a role at the cathode in Townsend-mechanism breakdown, however, is not so serious as it is in streamer-mechanism breakdown, and accordingly the calculations of the buildup of the transient Townsend discharge in our study suffer little changes in the general situation if we take into consideration the discharge not spreading over the whole surface of electrode in γ_p-predominant cases.

Table V shows the ratios of the values of quantities cited in the column (0) when the discharge is assumed to occupy a fractional part $(1/k)$ of the electrode surface, to those when it spreads over the whole surface. Column (I) gives the values under the condition that the externally supplied electron stream N_0 or initial current density J_0 is taken to be constant irrespective of discharge-spreading, and column (II), the values under the condition that the total number of externally supplied electrons per unit time N_0S or initial current I_0, is taken to be constant. In an electrode geometry such that the gap length is sufficiently small compared with the diameter of electrode, the discharge confines itself in a relatively small area instead of spreading over the electrode surface S_0 for γ_p-predominant processes. As a numerical example, let us take the discharge diameter to be 1 cm, a tenth of the electrode diameter. That is, $k=10^2$. Then under the condition (I), $\Delta_\rho\sigma$ remains as has been calculated above but $\Delta_I\sigma$ becomes one hundred times smaller, and conversely under the condition (II), $\Delta_I\sigma$ remains but $\Delta_\rho\sigma$ becomes ten thousand times larger. In both cases, $\Delta_\rho\sigma$ overtakes $\Delta_I\sigma$ at an earlier time T_0' than T_0 calculated above. Consequently, $\Delta_\rho\sigma$ and $\Delta_I\sigma$ are so small that $\Delta\sigma$ is nearly zero for $t<T_0'$ and the discharge can be sustained in γ_p-predominant cases as in γ_i-predominant cases.

TABLE V. Effect of discharge area on ionization integral.

(0)	(I)	(II)
J	1	k
$\Delta_\rho\sigma$	1	k^2
I	k^{-1}	1
$\Delta_I\sigma$	k^{-1}	1

Finally, at the last stage of formative time, localization will occur somewhere owing to high space-charge density and then a streamer having a narrower path than the discharge path in the formative time, will begin.

X. CONCLUSIONS

The following conclusions can be drawn from the results of the present study.

(i) The general solutions derived in PR1 are useful for computation of the space-charge distribution, space-charge distortion of field, growth of current, and change of ionization integral during the formative time of spark breakdown because the errors due to adoption of the finite terms are so small.

(ii) The growth of the transient Townsend discharge can be classified into γ_p-predominant cases and γ_i-predominant cases; the former correspond to $\lambda_{b1}>0$ and the latter, to $\lambda_{b1}<0$. The boundary of these regions, $\lambda_{b1}=0$, depends on γ_i, γ_p, and percent overvoltage Δ. The mode of development of space-charge distortion of field and growth of ionization in the discharge can be classified into γ_p-predominant and γ_i-predominant cases

in the same way as the development of space charges and the growth of currents.

(iii) In γ_p-predominant cases, a considerable space-charge accumulation and a sufficient current to drive the discharge into "glow" or "arc" are attained within the (b) range, but in γ_i-predominant cases they are not attained till the time passes into the (c) ranges.

(iv) The electronic space charges develop a steady-state-like distribution in the whole gap already in an early stage of the formative time of spark and the ionic space charges show such distribution only in the neighborhood of the anode. From this conclusion, it is clear that the expression for charge stream used by Bandel,[13] $N_+(x)=N_0(e^{\alpha l}-e^{\alpha x})$, which is completely valid only for a steady-state distribution set by under-voltage application, is approximately valid for a transient-state distribution in the (c) range, but not for a distribution in the (b) range.

(v) In view of these space-charge distributions in the formative time of spark, it may be concluded that anodic breakdown occurs in γ_p-predominant cases and cathodic breakdown, in γ_i-predominant cases.

(vi) Charge streams in the gap increases nearly proportionally to the discharge current except for smaller values of current.

(vii) In the initial stage of formative time of spark, the ionization integral takes a nearly constant value ($\bar{\alpha}l$) corresponding to an applied field $\bar{E}$, and in the middle stage it falls a little lower due to the potential drop in an external resistance; in the final stage it rises very rapidly due to the growth of space-charge distortion of field overcoming the negative effect of the potential drop in the resistance and reaches a critical value to advance the discharge into "glow." Such a sufficiently space-charge-distorted field and an ionization integral may be developed in some t_- or some tens of t_- in γ_p-predominant cases, but in several times $\bar{t}$ in γ_i-predominant cases.

(viii) Judging by the variation of the ionization integral with time, it can be said that the discharge spreads over the whole surface of the electrode in γ_i-predominant cases, but it spreads only over a fractional part of the cathode surface somewhat broader than an externally irradiated area in γ_p-predominant cases.

[13] $i_+(x)=i_0(e^{\alpha l}-e^{\alpha x})$ in Bandel's paper, p. 1125.

ACKNOWLEDGMENTS

The author wishes to express his gratitude to the late Professor S. Mochizuki of Osaka University, Honorary Professor K. Honda of Tokyo University, and Assistant Professor T. Mori of Keiogijuku University for their valuable suggestions and to Research Assistants Y. Fukuda and T. Suzuki and our students for their assistance in the numerical calculations. He also wishes to thank Professor L. B. Loeb of University of California for his interest in the problem and for several stimulating suggestions, and Dr. P. M. Davidson of University College of Swansea for his communication on the discussion of my previous paper. The present study has been supported by the Scientific Research Expenditure of the Ministry of Education (Japan) and Scientific Research Fund granted by the Asahi Press.